Csp^3–H Bond Activation Mediated by a Pd(II) Complex under Mild Conditions

Csp³–H Bond Activation Mediated by a Pd(II) Complex under Mild Conditions

Hanah Na,[a,b,#] Andrew J. Wessel,[c,#] Seoung-Tae Kim,[d,e,#] Mu-Hyun Baik,[d,e,*] and Liviu M. Mirica[a,*]

[a] Department of Chemistry, University of Illinois at Urbana-Champaign, 600 S. Mathews Avenue, Urbana, Illinois, 61801

[b] Current address: Center for Advanced Specialty Chemicals, Korea Research Institute of Chemical Technology (KRICT), Ulsan 44412, Republic of Korea

[c] Department of Chemistry, Washington University, St. Louis, Missouri, 63130-4899

[d] Department of Chemistry, Korea Advanced Institute of Science and Technology (KAIST), Daejeon 34141, Republic of Korea

[e] Center for Catalytic Hydrocarbon Functionalizations, Institute for Basic Science (IBS), Daejeon 34141, Republic of Korea

[#] These authors contributed equally

[*] Email: mbaik2805@kaist.ac.kr

[*] Email: mirica@illinois.edu

Abstract

In this work, we disclose a new pentadentate pyridinophane ligand, *N*-methyl-N'-(2-methylpyryl)-2,11-diaza[3.3](2,6)pyridinophane ($^{PicCH3}N4$), and its Pd(II) complexes. The reaction of the Pd precursor $[Pd^{II}(MeCN)_4]^{2+}$ with $^{PicCH3}N4$ leads to the formation of the palladacycle compound $[(^{PicCH2}N4)Pd^{II}]^+$ via an uncommon room-temperature Csp³–H bond activation at a Pd(II) metal center. The isolated complex was characterized by single-crystal X-ray diffraction, NMR spectroscopy, and cyclic voltammetry. Furthermore, various experimental investigations, including additive studies, kinetic isotope effect measurements, and Eyring analysis were carried out to probe the reaction kinetics and mechanism of the Csp³–H bond activation by the Pd(II) center. A combined experimental and theoretical mechanistic

analysis suggests that acetate-assisted Csp^3–H bond activation is preferred at high temperature, while both acetate-assisted and acetate-free Csp^3–H bond activation pathways are competitive at room temperature.

Introduction

The coordination chemistry of metal complexes supported by macrocyclic ligands has experienced great growth during the past several decades, as macrocyclic ligands can serve as models for biologically important species or impart thermodynamic and kinetic stability to their metal complexes in unusual oxidation states that are otherwise uncommon or metastable with the noncyclic ligand congeners.[1-7] Although a significant number of macrocyclic coordinating ligands for metal ions have been reported, developing new types of macrocyclic ligands is still an attractive goal for further applications and studies in the field of coordination chemistry. Among various macrocycles, the tetradentate *N,N'*-dialkyl-2,11-diaza[3.3](2,6)pyridinophane (^{R}N4, R = ^{t}Bu, ^{i}Pr, Me) ligands can serve as robust ligands for various metal ions (e. g., Pd, Ni, Cu, Co, Fe, Mn, Zn) and have been extensively investigated.[8-20] These tetradentate ^{R}N4 ligands provide unique environments to the coordinated metal center and enable various reactivity pathways for C–C/C–X bond formation,[11-12, 14, 16, 19-20] small molecule activation,[21-23] or water oxidation.[24-25] In contrast to tetradentate pyridinophane ligands, the reports on multidentate pyridinophane ligands with five or more donor atoms are sparse.[26-30] In order to explore new ligand scaffolds and investigate the related coordination chemistry, we report herein the synthesis of a new pentadentate pyridinophane ligand, *N*-methyl-N'-(2-methylpyryl)-2,11-diaza[3.3](2,6)pyridinophane (^{PicCH3}N4) and its Pd^{II} complexes. Interestingly, when the Pd^{II} precursor [Pd^{II}(MeCN)$_4$]$^{2+}$ was reacted with the ^{PicCH3}N4 ligand, the palladacycle compound [(^{PicCH2}N4)Pd^{II}]$^+$ was obtained, which formed via an uncommpn Csp^3–H activation of the ^{PicCH3}N4 ligand, under mild conditions and in absence of any base additive. The isolated complex was characterized by single-crystal X-ray

diffraction, NMR spectroscopy, and cyclic voltammetry. Furthermore, various experimental investigations, including additive studies, kinetic isotope effect measurements, and Eyring analysis were carried out to probe the reaction kinetics and mechanism of the Csp^3–H bond activation by the Pd(II) center. A combined experimental and theoretical mechanistic analysis suggests that acetate-assisted Csp^3–H bond activation is preferred at high temperature, while both acetate-assisted and acetate-free Csp^3–H bond activation pathways are competitive at room temperature. These results provide insights into the important process of Csp^3–H bond activation by Pd complexes that seems to be operative under mild conditions and without a base additive, and thus could be employed in a wider range of C-H functionalization reactions.

Results and discussion

Ligand synthesis. Our group has previously utilized the macrocyclic *N,N'*-dialkyl-2,11-diaza[3.3](2,6)pyridinophane (^{R}N4) ligands to study a variety of transition metal complexes.[8-15, 17-20, 31] As a continuation of our studies, we sought to further extend the denticity of the pyridinophane ligand framework through the attachment of a coordinating 2-methylpyridyl arm (2-picolyl, Pic), which results in a new type of pentadentate ligand, *N*-methyl-N'-(2-methylpyryl)-2,11-diaza[3.3](2,6)pyridinophane (^{PicCH3}N4, Scheme 1). The synthesis of ^{PicCH3}N4 started with the previously reported unsymmetric pyridinophane precursor, *N*-tosyl-2,11-diaza[3.3](2,6)pyridinophane (^{TsH}N4).[32] Addition of 2-(chloromethyl)-pyridine hydrochloride into ^{TsH}N4 with diisopropylethylamine in the presence of a catalytic amount of tetrabutylammonium bromide (TBABr) generated ^{TsPic}N4 in 89% yield. The detosylation and subsequent methylation through the Eschweiler-Clarke reaction afforded the desired ligand ^{PicCH3}N4 in 60% overall yield. In addition, the deuterated variant ^{PicCD3}N4, which was employed in mechanistic studies (see below), was synthesized through the Eschweiler-Clarke reaction of ^{PicH}N4 with 20% formaldehyde-d_2 in D_2O and formic acid-d_2. ^{1}H NMR spectroscopic analysis of the obtained ^{PicCD3}N4 ligand confirmed the absence of CH_3 functional group, while the ^{2}H

NMR spectrum clearly indicates the presence of CD_3 group (Figures S3 and S4).
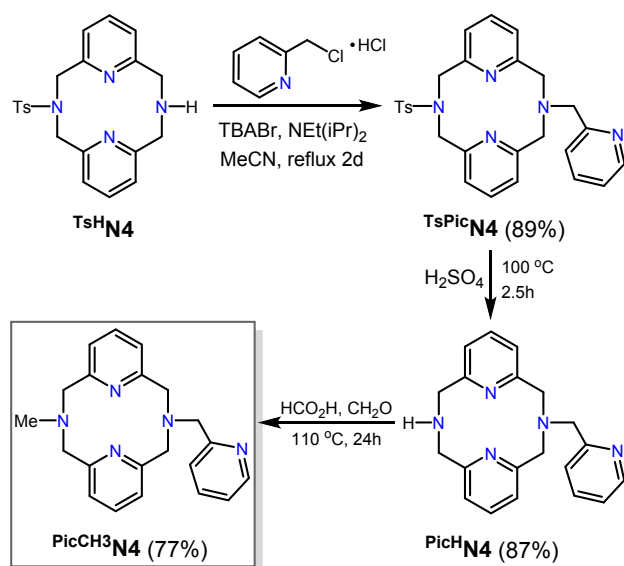

Scheme 1. Synthesis of newly developed ligand ^{PicCH3}N4.

Synthesis and characterization of Pd complexes. With the newly developed ligand in hand,

the synthesis of the corresponding Pd^{II} complex was attempted through the reaction of ^{PicCH3}N4

with $[Pd^{II}(MeCN)_4](BF_4)_2$ in MeCN at room temperature. Interestingly, the product obtained

from the reaction of ^{PicCH3}N4 with $[Pd^{II}(MeCN)_4]^{2+}$ was found to be an unexpected Pd complex,

$[(^{PicCH2}N4)Pd^{II}]^+$ (**1**), according to the single-crystal X-ray crystallography (Scheme 2 and

Figure 1) and ^1H NMR spectroscopic analysis (Figures S5–S9). Rather than the coordination

of N-donor atom in N–CH_3 arm, C–H activation of the methyl group by Pd resulted in the

formation of palladacycle **1**. Notably, the C–H activation occurs at room temperature, affording

1 in 40% yield, although the reaction requires 60 h. Warming up the reaction temperature to

50 °C marginally increased the yield of **1**, and heating at temperatures higher than 70 °C

resulted in decomposition. Instead, **1** can be obtained in a higher yield of 82% in the presence

of NaOAc and upon heating at 63 °C with significantly reduced reaction time (3 h, Scheme 2).

Complex **1** is a diamagnetic Pd^{II} species d^8 that was characterized by ^1H NMR spectroscopy. The evidence for C–H activation was supported by the absence of a chemical resonance corresponding to methyl protons (N-CH$_3$ at 2–3 ppm) and the presence of a downfield singlet corresponding to the methylene protons at 3.97 ppm (Figures S5–S9). X-ray quality crystals for **1** were obtained by slow diffusion of diethyl ether into a concentrated MeCN solution. X-ray crystal structure analysis of **1** reveals a square pyramidal geometry around the Pd^{II} center with the structural parameter $\tau_5 = 0.07$ (Figure 1, left).[33] The Pd–C bond distance of 2.017(2) Å is comparable to the previously reported values of Pd–C bond in palladacycles formed via C–H activation.[34-35] As the reaction of ^{PicCH3}N4 with $[Pd^{II}(MeCN)_4]^{2+}$ in the presence of NaOAc led to the formation of **1** in higher yield, we set out to probe whether a change of Pd precursor to Pd(OAc)$_2$ would readily generate **1**. However, the reaction of ^{PicCH3}N4 and Pd(OAc)$_2$ did not yield **1**, but instead afforded a four-coordinate acetate-bound Pd^{II} complex $[(^{PicCH3}N4)Pd^{II}(OAc)]^+$ (**2**), with one of the pyridine rings and the N–CH$_3$ donor atom not interacting with the Pd center (Scheme 2 and Figure 1). The C–H activation was not observed upon heating the reaction mixture up to 70 °C. In contrast to **1**, ^1H NMR spectrum of **2** exhibits a methyl peak (N–CH$_3$) chemical shift at 2.76 ppm, which is similar to those observed for several (^{Me}N4)Pd^{II} complexes, indicating that C–H activation did not occur in this case (Figure S10).[36-37] The structure of **2** reveals a square planar geometry of the Pd^{II} center, bonded to the three N donor atoms (two pyridine N atoms and one of the amine N atoms) of the ligand. The last coordination site is occupied by an acetate ligand, therefore positioning the methyl amine group far away (~4.4 Å) from the Pd metal center. These geometric considerations suggest that C–H activation is prevented due to the acetate binding, thus inhibiting an interaction between the Pd center and the C–H bond.
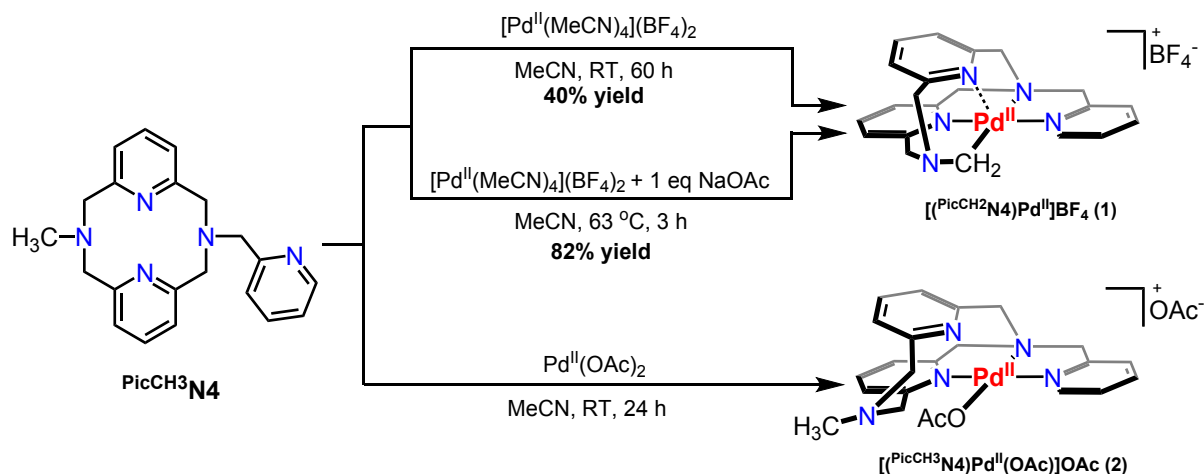
Scheme 2. Synthesis of Pd^{II} complexes.
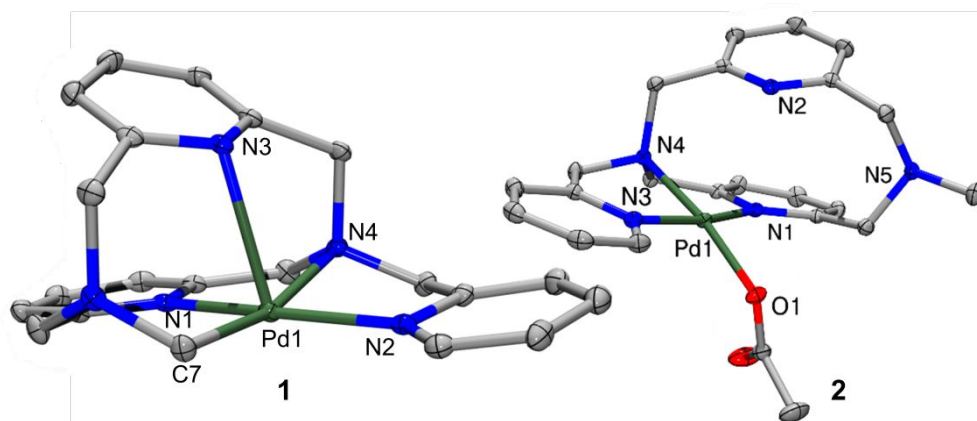
Figure 1. ORTEP representation of the cations of **1** (left) and **2** (right). Ellipsoids are shown at the 50% probability level with hydrogen atoms and counter ions are omitted for clarity. Selected bond distances (Å): **1**, Pd1–C7 2.017(2), Pd1–N1 2.0633(17), Pd1–N2 2.0695(18), Pd1–N3 2.5495(16), Pd1–N4 2.1677(16); **2**, Pd1–O1 2.0191(1), Pd1–N1 2.0432(1), Pd1–N3 1.9940(1), Pd1–N4 2.0220(1).

Electrochemical and Electron Paramagnetic Resonance (EPR) Studies. Due to the intriguing structure and the formation of **1**, its electrochemical properties were investigated by cyclic voltammetry (CV, Figure 2a). The CV of **1** in MeCN reveals an irreversible oxidation wave at 0.72 V vs Fc$^{+/0}$, which is assigned to the Pd$^{III/IV}$ couple. A pseudoreversible wave at –0.21 V vs Fc$^{+/0}$ likely corresponds to the Pd$^{II/III}$ couple, as observed previously for a related Pd^{II} complex (^{tBu}N4)PdMeCl.[37-38] When ^{PicCH3}N4 and [Pd^{II}(MeCN)$_4$]$^{2+}$ are mixed and analyzed *in-situ*, a different voltammogram profile was observed, indicating that the C–H activation of

the methyl group and the addition of the methylene donor ligand drastically changes the electrochemistry of the Pd^{II} complex (Figure S13). By contrast, the non C-H activated species $[(^{PicCH3})Pd^{II}]^{2+}$ exhibits higher oxidation events at 0.964 V vs $Fc^{+/0}$ and 1.20 V vs $Fc^{+/0}$, as expected for a Pd species with a higher overall charge. As the oxidation potential of **1** is chemically accessible, **1** was oxidized with 1 equiv ferrocenium tetrafluoroborate ($FcBF_4$) to generate a green species that is tentatively assigned as $[(^{PicCH2})N4Pd^{III}]^{2+}$. The EPR spectrum recorded at 77 K in 1:3 = MeCN:PrCN reveals a pseudoaxial signal with $g_x = 2.056$ ($A_x = 18$ G), $g_y = 2.083$, ($A_y = 19$ G), and $g_z = 2.277$ ($A_z = 5$ G) with superhyperfine coupling to three N atoms (Figure 2b). These g values are similar to those typically observed for Pd^{III} d^7 ions such as the ones in $(^{tBu}N4)Pd^{III}(X)_2$ or $(^{Me}N4)Pd^{III}(X)_2$ complexes.[39] However, the ordering of the g values ($g_z > g_x, g_y$) is different from that of most reported EPR spectra of six-coordinated mononuclear Pd^{III} complexes in a distorted octahedral geometry with a $(d_{z2})^1$ ground state.[40] This ordering of the g values is consistent with the Pd^{III} center with five-coordinate square pyramidal geometry and a $(d_{xy})^1$ or $(d_{x2-y2})^1$ ground state, as observed previously.[41] In addition, a splitting pattern due to the superhyperfine coupling to three N atoms with the Pd center is observed in both x and y directions, which is in line with a five-coordinate square pyramidal geometry. Gratifyingly, the DFT-calculated electronic structure and EPR parameters of the proposed $[(^{PicCH2})N4Pd^{III}]^{2+}$ species support a $(d_{x2-y2})^1$ ground state for this species, with the spin density localized mainly on the Pd center along with contributions from three N atoms (Figure S21). A similar splitting pattern in the x and y directions has been observed in the $[(N2S2)Pd^{III}MeCl]^+$ complex, which was suggested to have five-coordinate geometry with N atoms in the equatorial plane.[41]
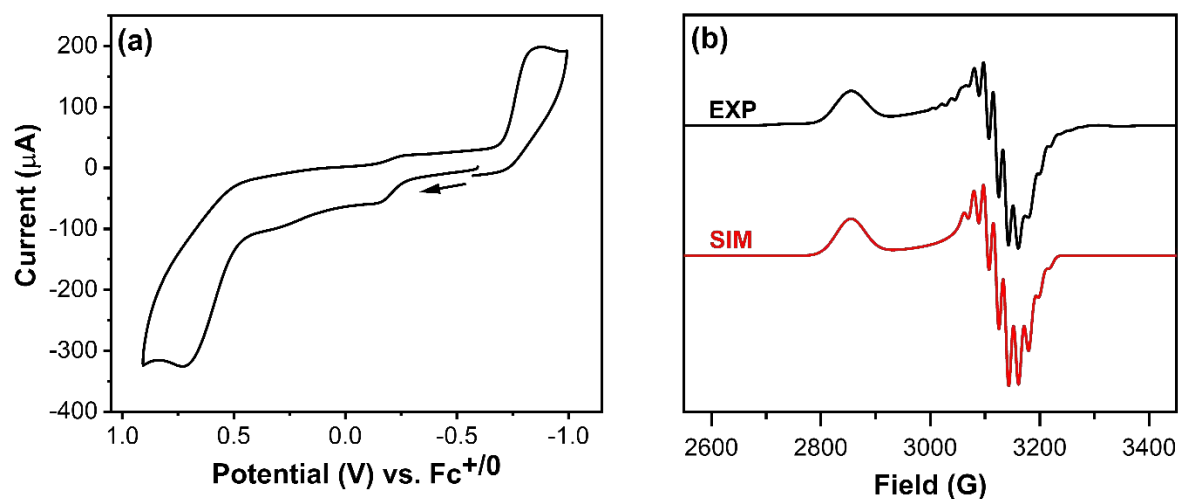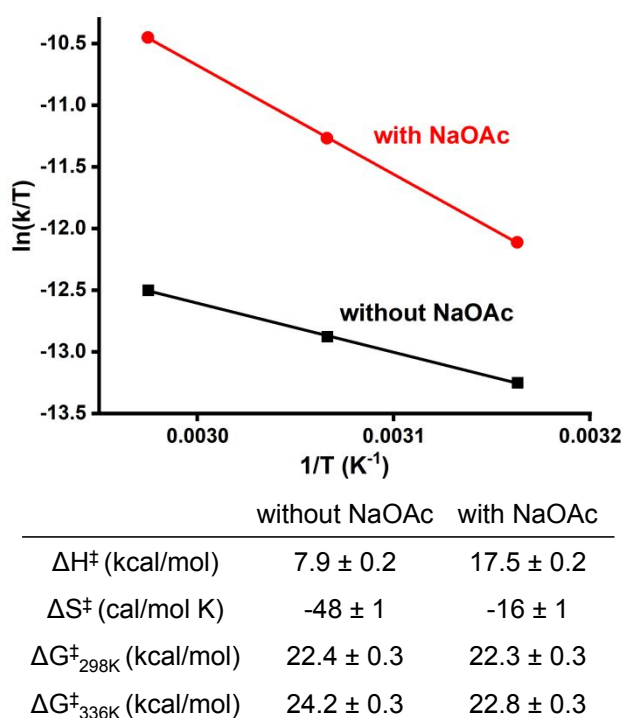
Figure 2. (a) Cyclic voltammogram (CV) of **1** in 0.1 M Bu$_4$NClO$_4$/MeCN (scan rate 0.1 V/s). (b) EPR spectrum (black line) of **1** after treating with 1 equiv. of FcBF$_4$ in 1:3 MeCN:PrCN glass at 77 K. The following g values were used for the simulation (red line): g_x = 2.056 (A$_x$ = 18 G), g_y = 2.083, (A$_y$ = 19 G), and g_z = 2.277 (A$_z$ = 5 G).

Effect of additives on C–H bond activation. The observed Csp^3–H activation and formation of **1** prompted us to investigate its kinetics and reaction mechanism. First, since it is commonly known that a base additive (e.g., acetate) can promote the C–H activation step via a concerted metalation-deprotonation (CMD) process,[42-48] we have investigated the effect of various additives on the formation of **1**. The addition of 1 equiv NaOAc to the reaction mixture at room temperature did not significantly increase the product yield, however, increasing the reaction temperature to 63°C led to an appreciable increase in yield of **1** up to 82% within 3 h. Since this reaction condition yielded a fast and clean formation of **1**, the kinetic isotope effects (KIE) measurements were performed with 1 equiv NaOAc at 63°C, as discussed in the next section. By comparison, the addition of 1 equiv of 1,8-bis(dimethylamino)naphthalene (proton sponge), lithium hexamethyldisilazide (LiHMDS), tetramethylammonium mesylamide (NMe$_4$MsNH), cesium pivalate (CsOPiv), silver acetate (AgOAc), or tetrabutylammonium acetate (TBAOAc) failed to induce C–H bond activation by the Pd^{II} center, complex decomposition occurring instead (Table S2). In addition, use of other Pd precursors such as Pd(OAc)$_2$ or Pd(TFA)$_2$ did not lead to any C-H bond activation of ^{PicCH3}N4. Considering the higher solubility of CsOPiv,

AgOAc, and TBAOAc compared to that of NaOAc, we suspect that stable acetate-coordinated Pd species are preferably formed with these soluble acetate salts and this leads to inhibition of C–H activation, as seen in the case when $Pd(OAc)_2$ was used as the precursor (Scheme 2 and Table S2). Given these observations, a substoichiometric amount of TBAOAc was employed, and addition of 0.5 equiv TBAOAc generates **1** in 80% yield in 3 h (Table S2). This result further supports our hypothesis that a stoichiometric or excess amount of acetate present in solution inhibits C–H activation due to the competing acetate binding to the Pd metal center, generating a coordinatively saturated species in which no weak interaction between the C–H and the Pd center is possible. In addition, the formation of **1** in the presence of acetate seems to require the dissociation of acetate from the Pd complex – which can be achieved at higher temperatures, in order to allow a weak interaction between the Pd metal center and the C–H bond that precedes C–H activation.

Reaction kinetics and thermodynamics. To gain insight into the C–H activation process, kinetic isotope effects (KIE) measurements were performed. The formation of **1** upon the reaction of $[Pd(MeCN)_4]^{2+}$ with $^{Pic}CH_3N4$ or $^{Pic}CD_3N4$ ligand in the presence of NaOAc in CD_3CN at 63 °C was monitored using ^1H and ^2H NMR, respectively (Figures S14 and S15). Since the full conversion to the C-H activated product was not achieved under these conditions, the initial rates method was employed to compare the deuterated vs. the non-deuterated ligand. The initial rates were determined for the formation of the C–H activated product by monitoring the growth of the Pd–C*H2*– peaks for $^{Pic}CH_3N4$ and the Pd–C*D2*– peaks for $^{Pic}CD_3N4$, to give rates of 0.0153 ± 0.0003 M h^{-1} and 0.0067 ± 0.0011 M h^{-1}, respectively. These initial rates correspond to a KIE value of 2.3 ± 0.4 (Figure S16 and Table S1), suggesting that the C–H bond cleavage step is at least partially rate-limiting, and in line with previous KIE values obtained for Pd-mediated C–H bond activation processes occurring via a CMD mechanism.[42-43, 49-52] To obtain further insight, we have performed an Eyring analysis via the initial rate

method, by measuring the initial rates of formation of **1** at three different reaction temperatures (43 °C, 53 °C, and 63 °C), in the absence or presence of the NaOAc additive. Analysis of the temperature dependence of the initial rates resulted in a straight line that gave the activation parameters $\Delta H^{\ddagger} = 7.9 \pm 0.2$ kcal/mol and $\Delta S^{\ddagger} = -48 \pm 1$ cal/mol·K in the absence of NaOAc, and $\Delta H^{\ddagger} = 17.5 \pm 0.2$ kcal/mol and $\Delta S^{\ddagger} = -16 \pm 1$ cal/mol·K in the presence of NaOAc (Figures 3 and S17). Without NaOAc, a large negative entropy of activation ($\Delta S^{\ddagger}$) was obtained, suggesting a possible bimolecular reaction. This correlates well with the DFT-calculated transition state that involves a deprotonation step assisted by the pyridyl group of another $^{PicCH3}N4$ ligand (see below, Figure 4). On the other hand, in the presence of NaOAc a smaller negative $\Delta S^{\ddagger}$ value is obtained, suggesting an ordered transition state in which the C–H bond activation step is promoted by the pre-coordinated acetate, akin to a typical CMD mechamism.[42-45, 51-52] Interestingly, at room temperature a Gibbs activation energy of $\Delta G^{\ddagger} = 22.4$ kcal/mol was obtained in the reaction without NaOAc, which is virtually identical to that obtained in the presence of NaOAc ($\Delta G^{\ddagger} = 22.3$ kcal/mol). However, at 63 °C a value of $\Delta G^{\ddagger} = 22.8$ kcal/mol was obtained for the reaction with NaOAc, which is significantly lower than that of the reaction without NaOAc ($\Delta G^{\ddagger} = 24.2$ kcal/mol). These results are in line with the increased yield of **1** obtained in a shorter time with NaOAc at elevated temperatures, as observed experimentally, and support the general conditions employed in Pd-mediated C-H bond activation that employ acetate additives and elevated temperatures. In addition, these results also reveal an important finding that acetate-free C–H bond activation by Pd centers can occur at room temperature, especially ~~in~~ in cases in which the presence of acetate may block all coordination sites of the Pd center. Overall, the presence of a coordinating base that can promote a CMD mechanism seems to favor entropically the rate of C–H bond activation, and the base is also needed for neutralizing the generated protons and increase the overall C–H activated product yield.

	without NaOAc	with NaOAc
$\Delta H^{\ddagger}$ (kcal/mol)	7.9 ± 0.2	17.5 ± 0.2
$\Delta S^{\ddagger}$ (cal/mol K)	-48 ± 1	-16 ± 1
$\Delta G^{\ddagger}_{298K}$ (kcal/mol)	22.4 ± 0.3	22.3 ± 0.3
$\Delta G^{\ddagger}_{336K}$ (kcal/mol)	24.2 ± 0.3	22.8 ± 0.3

Figure 3. Eyring plot for the generation of **1** obtained from the growth of methylene peak (Pd–CH_2) and activation parameters obtained from Eyring analysis.

DFT calculations. With these experimental results in hand, we then performed density functional theory (DFT) calculations to provide support for the proposed reaction mechanism. All calculations were performed by employing the B3LYP-D3/LACVP/6-31G** level of theory for the geometry optimization, vibrational analysis, and solvation energy calculations. The electronic energies of all optimized structures were reevaluated with B3LYP-D3/LACV3P/cc-pVTZ(-f), and further computational details are given in the Supporting information. The energy profile of the proposed reaction mechanism in the absence of acetate additive is shown in Figure 4.

11
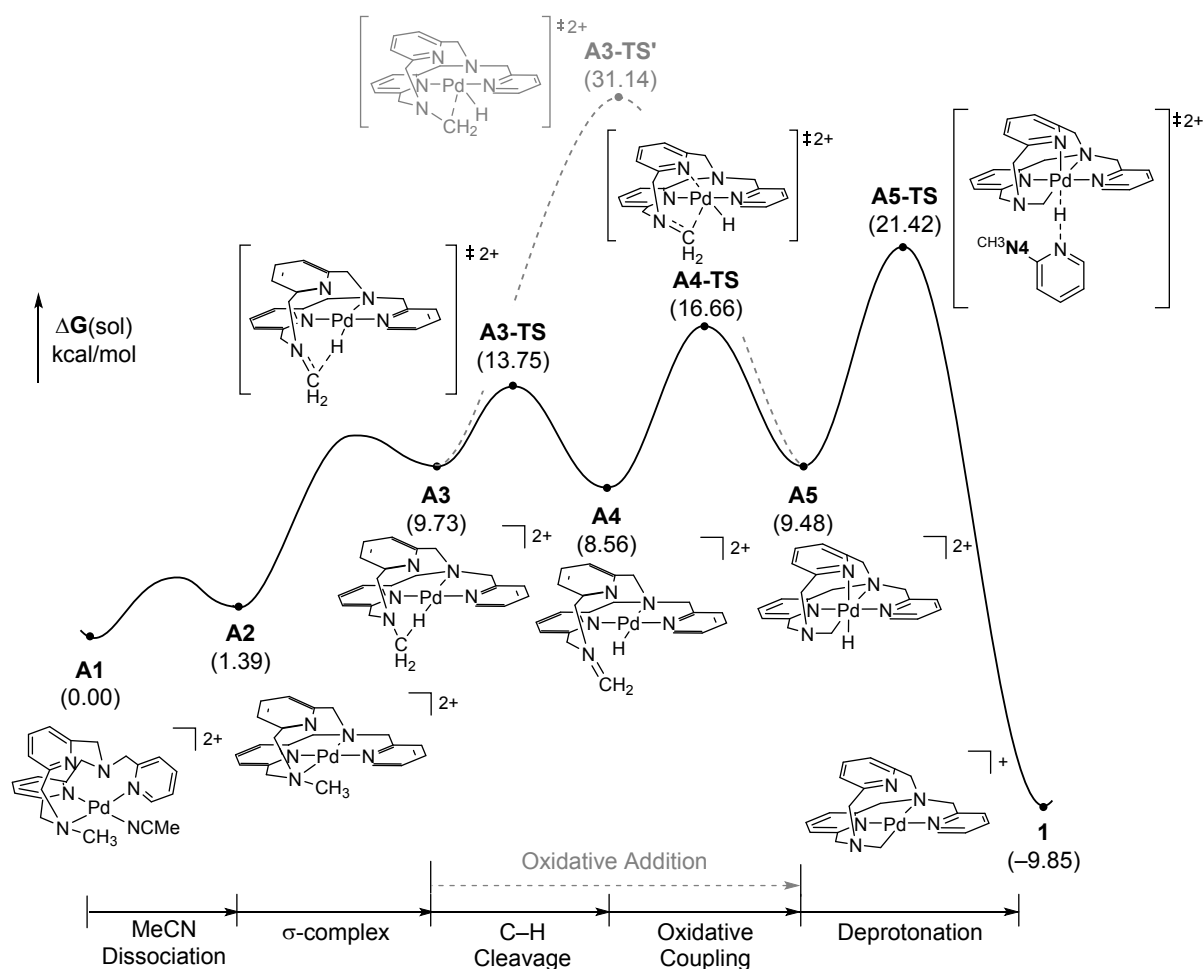
Figure 4. DFT-calculated energy profile for the Pd-mediated C–H activation of $^{PicCH3}N4$, describing the reaction mechanism of generating **1** in the absence of acetate additive.

The reaction initiates with the formation of σ-complex (**A3**), which is located at 9.7 kcal/mol higher energy than the unactivated ($^{PicCH3}N4$)Pd species. Next, the Csp^3–H bond of **A3** is cleaved through the **A3-TS** transition state that has a barrier of 13.8 kcal/mol, which involves a hydride abstraction to generate a Pd-hydride species and a methyleneiminium intermediate **A4**. The methyleneiminium carbocation then undergoes oxidative addition to the Pd center, leading to the formation of a Pd(IV) species **A5** at 9.5 kcal/mol via a transition state **A4-TS** with a barrier of 16.7 kcal/mol. This stepwise C–H activation process is expected to be more facile than the concerted mechanism, which involves C–H cleavage through oxidative addition *via* **A3-TS'**, with a barrier of 31.1 kcal/mol.[44-45, 51-53] Finally, **A5** is reduced through

deprotonation by the pyridyl group of another $^{PicCH3}N4$ ligand *via* **A5-TS** that has the highest

barrier of the overall reaction at 21.4 kcal/mol, to ultimately generate observed product **1** at –

9.9 kcal/mol. Importantly, since a second equivalent of $^{PicCH3}N4$ is acting as base to remove the

proton formed upon C–H cleavage, the yield of **1** is expected to be lower than 50%, which is

consistent with the experimental result, along with the formation of protonated $^{PicCH3}N4$ ligand

(Table S2). In addition, this bimolecular rate-determining step is expected to have a large

negative entropy of activation, which is exactly what was obtained experimentally from the

Eyring analysis (Figure 3).
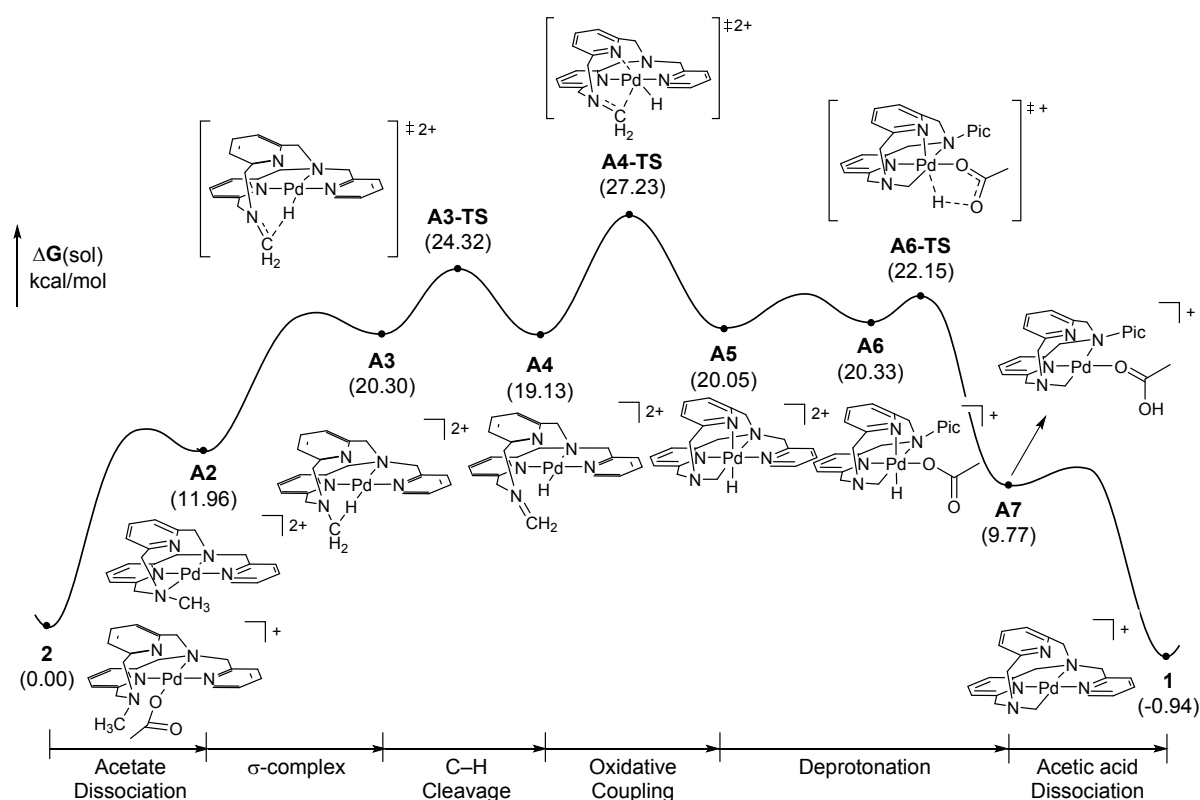
Figure 5. DFT-calculated energy profile for the Pd-mediated C–H activation of $^{PicCH3}N4$, describing the reaction mechanism of generating **1** in the presence of acetate additive.

Figure 5 summarizes the results of examining the mechanism for the formation of **1** in

the presence of acetate. The calculations suggest that the Pd-acetate complex **2** is the resting

state of the reaction in the presence of acetate. Complex **2** is 10.6 kcal/mol more stable than

A1, the resting state of the reaction without acetate, resulting in an increased overall barrier for the oxidative addition of 27.2 kcal/mol, despite the C–H activation mechanism being identical to that proposed for the reaction without acetate present (Figure 4). Moreover, the dramatically increased yield of C-H activation product formed in the presence of 0.5 equiv vs. 1 equiv TBAOAc further supports that acetate dissociation is needed for generating a coordinatively unsaturated species in which a weak interaction between the C–H bond and the Pd center is possible. These results also indicate that the reaction in the presence of acetate may require a higher reaction temperature. An alternate mechanism was also considered, that is the conventional concerted metalation-deprotonation (CMD) process in which the Pd-bound acetate promotes the C–H activation.[51-52] However, the calculations suggest the CMD process is not feasible as it has an insurmountable barrier of 37.1 kcal/mol, and likely due to the repulsion between the lone pair of the axial pyridine N atom and the d_{z^2} orbital of the Pd center (Figure S20). After oxidative addition to generate the Pd(IV) intermediate **A5**, acetate binding would generate **A6**, followed by acetate-assisted deprotonation *via* the **A6-TS** transition state at 22.2 kcal/mol. Finally, the dissociation of acetic acid at **A7** leads to the desired product **1**. Overall, the proposed mechanism implies that in the presence of acetate the yield is not limited to < 50%, in line with the experimental results that show an improved yield of **1** at higher temperatures in the presence of acetate (Scheme 2). Moreover, the ordered **A4-TS** rate-limiting transition state, formed via a unimolecular reaction, is expected to correspond to a small, negative entropy of activation, in line with the Eyring analysis result (Figure 3). Finally, while the acetate-free pathway was calculated to have a transition state that is 5.81 kcal/mol lower in energy than the pathway calculated in presence of acetate, the experimental results suggest comparable rates for both pathways. However, it is important to keep in mind that the acetate-free pathway is proposed to adopt a bimolecular mechanism that will be significantly influenced entropically by the concentrations employed in these reactions, while the

calculations assumed a 1 M standard state in solution. Moreover, the activation energy for the acetate-mediated deprotonation step corresponding to the **A6-TS** transition state could be higher than calculated, since the concentration of acetate is significantly lower than 1 M; such a higher energy **A6-TS** transition state could also support the experimental determined KIE value that deviates from 1.

Conclusion

In conclusion, herein we report a new pentadentate pyridinophane ligand $^{PicCH3}N4$ and its Pd^{II} complexes. The reaction of the Pd precursor $[Pd^{II}(MeCN)_4]^{2+}$ with $^{PicCH3}N4$ gave $[(^{PicCH2}N4)Pd^{II}]^+$ (**1**), which formed from the uncommon Csp^3–H activation by Pd^{II} occurring at room temperature. Complex **1** was isolated and characterized by single-crystal X-ray crystallography, NMR, cyclic voltammetry, as well as the EPR characterization of the related one-electron oxidized Pd^{III} species. In addition, various experimental investigations such as KIE measurements and Eyring analysis were conducted to understand the reaction kinetics and mechanism of the Csp^3–H bond activation by Pd^{II} center. Through a detailed mechanistic analysis, we show that acetate-assisted C–H bond activation is preferred at higher temperatures, although acetate-free C–H bond activation can be competitive at room temperature, and thus can occur under milder conditions than initially anticipated. Overall, the newly developed macrocyclic pentadentate pyridinophane framework presented herein provides further impetus to explore its applications in coordination chemistry, form organometallic catalysis to bioinorganic chemistry.

Corresponding Authors

Liviu M. Mirica – Department of Chemistry, University of Illinois at Urbana-Champaign, 600 S. Mathews Avenue, Urbana, IL, 61801, USA

Email: mirica@illinois.edu

Mu-Hyun Baik – Center for Catalytic Hydrocarbon Functionalizations, Institute for Basic Science (IBS), Daejeon 34141, Republic of Korea; Department of Chemistry, Korea Advanced Institute of Science and Technology (KAIST), Daejeon 34141, Republic of Korea

Email: mbaik2805@kaist.ac.kr

Authors

Hanah Na – Department of Chemistry, University of Illinois-Urbana Champaign, 600 S. Mathews Avenue, Urbana, IL, 61801, USA

Andrew J. Wessel – Department of Chemistry, Washington University, St. Louis, Missouri, 63130, USA

Seoung-Tae Kim – Department of Chemistry, Korea Advanced Institute of Science and Technology (KAIST), Daejeon 34141, Republic of Korea; Center for Catalytic Hydrocarbon Functionalizations, Institute for Basic Science (IBS), Daejeon 34141, Republic of Korea

ORCID

Hanah Na: 0000-0002-0576-4806

Andrew J. Wessel: 0000-0003-2012-3596

Seoung-Tae Kim: 0000-0003-4067-9567

Mu-Hyun Baik: 0000-0002-8832-8187

Liviu M. Mirica: 0000-0003-0584-9508

Acknowledgments

References

1. G. Melson, *Coordination chemistry of macrocyclic compounds*, Springer Science & Business Media, 2012.

2. S. J. Archibald, Coordination chemistry of macrocyclic ligands, *Annu. Rep. Prog. Chem., Sect. A: Inorg. Chem.*, 2009, **105**, 297-322.

3. A. Haque, R. Ilmi, I. J. Al-Busaidi and M. S. Khan, Coordination chemistry and application of mono- and oligopyridine-based macrocycles, *Coord. Chem. Rev.*, 2017, **350**, 320-339.

4. R. E. Mewis and S. J. Archibald, Biomedical applications of macrocyclic ligand complexes, *Coord. Chem. Rev.*, 2010, **254**, 1686-1712.

5. T. Joshi, B. Graham and L. Spiccia, Macrocyclic Metal Complexes for Metalloenzyme Mimicry and Sensor Development, *Acc. Chem. Res.*, 2015, **48**, 2366-2379.

6. L. Fabbrizzi, The Stabilization of High Oxidation States of Metals Through Coordination by Poly-aza Macrocycles, *Comments Inorg. Chem.*, 1985, **4**, 33-54.

7. M. Jagoda, S. Warzeska, H. Pritzkow, H. Wadepohl, P. Imhof, J. C. Smith and R. Krämer, Catalytic Transesterification of Dialkyl Phosphates by a Bioinspired Dicopper(II) Macrocyclic Complex, *J. Am. Chem. Soc.*, 2005, **127**, 15061-15070.

8. W. O. Koch and H.-J. Krüger, A Highly Reactive and Catalytically Active Model System for Intradiol-Cleaving Catechol Dioxygenases: Structure and Reactivity of Iron(III) Catecholate Complexes of N,N′-Dimethyl-2,11-diaza[3.3](2,6)pyridinophane, *Angew. Chem., Int. Ed.*, 1995, **34**, 2671-2674.

9. W. O. Koch, A. Barbieri, M. Grodzicki, V. Schünemann, A. X. Trautwein and H.-J. Krüger, Eight Coordinate Iron(II) and Iron(III) Ions in Complexes with Distorted Dodecahedral FeN8 Environments: Synthesis and Structures of Bis(2,11-diaza[3.3](2,6)pyridinophane0iron Complexes, *Angew. Chem., Int. Ed.*, 1996, **35**, 422-424.

10. M. Graf, G. Wolmershäuser, H. Kelm, S. Demeschko, F. Meyer and H.-J. Krüger, Temperature-Induced Spin-Transition in a Low-Spin Cobalt(II) Semiquinonate Complex, *Angew. Chem., Int. Ed.*, 2010, **49**, 950-953.

11. J. R. Khusnutdinova, N. P. Rath and L. M. Mirica, Stable Mononuclear Organometallic Pd(III) Complexes and Their C-C Bond Formation Reactivity, *J. Am. Chem. Soc.*, 2010, **132**, 7303-7305.

12. T. W.-S. Chow, E. L.-M. Wong, Z. Guo, Y. Liu, J.-S. Huang and C.-M. Che, cis-

Dihydroxylation of Alkenes with Oxone Catalyzed by Iron Complexes of a Macrocyclic Tetraaza Ligand and Reaction Mechanism by ESI-MS Spectrometry and DFT Calculations, *J. Am. Chem. Soc.*, 2010, **132**, 13229-13239.

13.   J. R. Khusnutdinova, N. P. Rath and L. M. Mirica, The Aerobic Oxidation of a Pd(II) Dimethyl Complex Leads to Selective Ethane Elimination from a Pd(III) Intermediate, *J. Am. Chem. Soc.*, 2012, **134**, 2414-2422.

14.   F. Z. Tang, Y. Zhang, N. P. Rath and L. M. Mirica, Detection of Pd(III) and Pd(IV) Intermediates during the Aerobic Oxidative C-C Bond Formation from a Pd(II) Dimethyl Complex, *Organometallics*, 2012, **31**, 6690-6696.

15.   J. R. Khusnutdinova, J. Luo, N. P. Rath and L. M. Mirica, Late First-Row Transition Metal Complexes of a Tetradentate Pyridinophane Ligand: Electronic Properties and Reactivity Implications, *Inorg. Chem.*, 2013, **52**, 3920-3932.

16.   B. Zheng, F. Z. Tang, J. Luo, J. W. Schultz, N. P. Rath and L. M. Mirica, Organometallic Nickel(III) Complexes Relevant to Cross-Coupling and Carbon-Heteroatom Bond Formation Reactions, *J. Am. Chem. Soc.*, 2014, **136**, 6499-6504.

17.   F. Z. Tang, N. P. Rath and L. M. Mirica, Stable bis(trifluoromethyl)nickel(III) complexes, *Chem Commun*, 2015, **51**, 3113-3116.

18.   F. S. Menges, S. M. Craig, N. Tötsch, A. Bloomfield, S. Ghosh, H.-J. Krüger and M. A. Johnson, Capture of CO2 by a Cationic Nickel(I) Complex in the Gas Phase and Characterization of the Bound, Activated CO2 Molecule by Cryogenic Ion Vibrational Predissociation Spectroscopy, *Angew. Chem., Int. Ed.*, 2016, **55**, 1282-1285.

19.   J. W. Schultz, K. Fuchigami, B. Zheng, N. P. Rath and L. M. Mirica, Isolated Organometallic Nickel(III) and Nickel(IV) Complexes Relevant to Carbon-Carbon Bond Formation Reactions, *J. Am. Chem. Soc.*, 2016, **138**, 12928–12934.

20.   J. Serrano-Plana, A. Aguinaco, R. Belda, E. García-España, M. G. Basallote, A. Company and M. Costas, Exceedingly Fast Oxygen Atom Transfer to Olefins via a Catalytically Competent Nonheme Iron Species, *Angew. Chem., Int. Ed.*, 2016, **55**, 6310-6314.

21.   D. Jeong, T. Ohta and J. Cho, Structure and Reactivity of a Mononuclear Nonheme Manganese(III)–Iodosylarene Complex, *J. Am. Chem. Soc.*, 2018, **140**, 16037-16041.

22.   K. Kim, D. Cho, H. Noh, T. Ohta, M.-H. Baik and J. Cho, Controlled Regulation of the Nitrile Activation of a Peroxocobalt(III) Complex with Redox-Inactive Lewis Acidic Metals, *J. Am. Chem. Soc.*, 2021, **143**, 11382-11392.

23.   H. Sugimoto, K. Ashikari and S. Itoh, C–H Bond Activation of the Methyl Group of the Supporting Ligand in an Osmium(III) Complex upon Reaction with H2O2: Formation of

an Organometallic Osmium(IV) Complex, *Inorg. Chem.*, 2013, **52**, 543-545.

24. W.-T. Lee, S. B. Muñoz Iii, D. A. Dickie and J. M. Smith, Ligand Modification Transforms a Catalase Mimic into a Water Oxidation Catalyst, *Angew. Chem., Int. Ed.*, 2014, **53**, 9856-9859.

25. W.-P. To, T. Wai-Shan Chow, C.-W. Tse, X. Guan, J.-S. Huang and C.-M. Che, Water oxidation catalysed by iron complex of N,N[prime or minute]-dimethyl-2,11-diaza[3,3](2,6)pyridinophane. Spectroscopy of iron-oxo intermediates and density functional theory calculations, *Chem. Sci.*, 2015, **6**, 5891-5903.

26. A. Roca-Sabio, C. S. Bonnet, M. Mato-Iglesias, D. Esteban-Gómez, É. Tóth, A. d. Blas, T. Rodríguez-Blas and C. Platas-Iglesias, Lanthanide Complexes Based on a Diazapyridinophane Platform Containing Picolinate Pendants, *Inorg. Chem.*, 2012, **51**, 10893-10903.

27. G. Castro, R. Bastida, A. Macías, P. Pérez-Lourido, C. Platas-Iglesias and L. Valencia, Pyridinophane Platform for Stable Lanthanide(III) Complexation, *Inorg. Chem.*, 2013, **52**, 6062-6072.

28. N. Bandara, A. K. Sharma, S. Krieger, J. W. Schultz, B. H. Han, B. E. Rogers and L. M. Mirica, Evaluation of ^{64}Cu-based Radiopharmaceuticals That Target Aβ Peptide Aggregates as Diagnostic Tools for Alzheimer's Disease, *J. Am. Chem. Soc.*, 2017, **139**, 12550-12558.

29. A. K. Sharma, J. W. Schultz, J. T. Prior, N. P. Rath and L. M. Mirica, Coordination Chemistry of Bifunctional Chemical Agents Designed for Applications in ^{64}Cu PET Imaging for Alzheimer's Disease, *Inorg. Chem.*, 2017, **56**, 13801-13814.

30. Y. Huang, T. T. Huynh, L. Sun, C.-H. Hu, Y.-C. Wang, B. E. Rogers and L. M. Mirica, Neutral Ligands as Potential [64]Cu Chelators for Positron Emission Tomography Imaging Applications in Alzheimer's Disease, *Inorg. Chem.*, 2022, **61**, 4778–4787.

31. B. Zheng, F. Tang, J. Luo, J. W. Schultz, N. P. Rath and L. M. Mirica, Organometallic Nickel(III) Complexes Relevant to Cross-Coupling and Carbon–Heteroatom Bond Formation Reactions, *J. Am. Chem. Soc.*, 2014, **136**, 6499-6504.

32. A. J. Wessel, J. W. Schultz, F. Tang, H. Duan and L. M. Mirica, Improved synthesis of symmetrically & asymmetrically N-substituted pyridinophane derivatives, *Org. Biomol. Chem.*, 2017, **15**, 9923-9931.

33. A. W. Addison, T. N. Rao, J. Reedijk, J. van Rijn and G. C. Verschoor, Synthesis, structure, and spectroscopic properties of copper(ii) compounds containing nitrogen sulfur donor ligands - the crystal and molecular-structure of aqua[1,7-bis(n-

methylbenzimidazol-2'-yl)-2,6-dithiaheptane]copper(ii) perchlorate, *J. Chem. Soc., Dalton Trans.*, 1984, 1349-1356.

34.   P. Halder, D. J. SantaLucia, S. V. Park and J. F. Berry, From Pincer to Paddlewheel: C–H and C–S Bond Activation at Bis(2-pyridylthio)methane by Palladium(II), *Inorg. Chem.*, 2019, **58**, 2270-2274.

35.   W. H. Henderson, J. M. Alvarez, C. C. Eichman and J. P. Stambuli, Characterization, Reactivity, and Potential Catalytic Intermediacy of a Cyclometalated Tri-tert-butylphosphine Palladium Acetate Complex, *Organometallics*, 2011, **30**, 5038-5044.

36.   F. Tang, Y. Zhang, N. P. Rath and L. M. Mirica, Detection of Pd(III) and Pd(IV) Intermediates during the Aerobic Oxidative C-C Bond Formation from a Pd(II) Dimethyl Complex, *Organometallics*, 2012, **31**, 6690-6696.

37.   F. Tang, F. Qu, J. R. Khusnutdinova, N. P. Rath and L. M. Mirica, Structural and Reactivity Comparison of Analogous Organometallic Pd(III) and Pd(IV) Complexes, *Dalton Trans.*, 2012, **41**, 14046-14050.

38.   J. R. Khusnutdinova, N. P. Rath and L. M. Mirica, The Conformational Flexibility of the Tetradentate Ligand tBuN4 is Essential for the Stabilization of (tBuN4)PdIII Complexes, *Inorg. Chem.*, 2014, **53**, 13112-13129.

39.   F. Z. Tang, S. V. Park, N. P. Rath and L. M. Mirica, Electronic versus steric effects of pyridinophane ligands on Pd(III) complexes, *Dalton Trans.*, 2018, **47**, 1151-1158.

40.   J. R. Khusnutdinova and L. M. Mirica, in *C-H and C-X Bond Functionalization: Transition Metal Mediation*, ed. X. Ribas, Royal Society of Chemistry, 2013, DOI: 10.1039/9781849737166-00122 ch. 5, pp. 122-158.

41.   J. Luo, N. P. Rath and L. M. Mirica, Oxidative Reactivity of (N2S2)PdRX Complexes (R = Me, Cl; X = Me, Cl, Br): Involvement of Palladium(III) and Palladium(IV) Intermediates, *Organometallics*, 2013, **31**, 3343-3353.

42.   A. D. Ryabov, I. K. Sakodinskaya and A. K. Yatsimirsky, Kinetics and mechanism of ortho-palladation of ring-substituted NN-dimethylbenzylamines, *J. Chem Soc., Dalton Trans.*, 1985, **14**, 2629-2638.

43.   A. D. Ryabov, Mechanisms of intramolecular activation of carbon-hydrogen bonds in transition-metal complexes, *Chem. Rev.*, 1990, **90**, 403-424.

44.   M. Lafrance and K. Fagnou, Palladium-Catalyzed Benzene Arylation: Incorporation of Catalytic Pivalic Acid as a Proton Shuttle and a Key Element in Catalyst Design, *J. Am. Chem. Soc.*, 2006, **128**, 16496-16497.

45.   D. Lapointe and K. Fagnou, Overview of the Mechanistic Work on the Concerted

Metallation–Deprotonation Pathway, *Chem. Lett.*, 2010, **39**, 1118-1126.

46. T. W. Lyons and M. S. Sanford, Palladium-Catalyzed Ligand-Directed C-H Functionalization Reactions, *Chem. Rev.*, 2010, **110**, 1147-1169.

47. L. Ackermann, Carboxylate-Assisted Transition-Metal-Catalyzed C−H Bond Functionalizations: Mechanism and Scope, *Chem. Rev.*, 2011, **111**, 1315-1345.

48. J. He, M. Wasa, K. S. L. Chan, Q. Shao and J.-Q. Yu, Palladium-Catalyzed Transformations of Alkyl C–H Bonds, *Chem. Rev.*, 2017, **117**, 8754-8786.

49. E. M. Simmons and J. F. Hartwig, On the Interpretation of Deuterium Kinetic Isotope Effects in C☐H Bond Functionalizations by Transition-Metal Complexes, *Angew. Chem., Int. Ed.*, 2012, **51**, 3066-3072.

50. M. Gomez-Gallego and M. A. Sierra, Kinetic Isotope Effects in the Study of Organometallic Reaction Mechanisms, *Chem. Rev.*, 2011, **111**, 4857-4963.

51. D. L. Davies, S. M. A. Donald and S. A. Macgregor, Computational Study of the Mechanism of Cyclometalation by Palladium Acetate, *J. Am. Chem. Soc.*, 2005, **127**, 13754-13755.

52. D. L. Davies, S. A. Macgregor and C. L. McMullin, Computational Studies of Carboxylate-Assisted C–H Activation and Functionalization at Group 8–10 Transition Metal Centers, *Chem. Rev.*, 2017, **117**, 8649-8709.

53. D. Balcells, E. Clot and O. Eisenstein, C—H Bond Activation in Transition Metal Species from a Computational Perspective, *Chem. Rev.*, 2010, **110**, 749-823.

Csp³–H Bond Activation Mediated by a Pd(II) Complex under Mild Conditions

Hanah Na,[a,b,#] Andrew J. Wessel,[c,#] Seoung-Tae Kim,[d,e,#] Mu-Hyun Baik,[d,e,*] and Liviu M. Mirica[a, *]

[a] Department of Chemistry, University of Illinois at Urbana-Champaign, 600 S. Mathews Avenue, Urbana, Illinois, 61801

[b] Current address: Center for Advanced Specialty Chemicals, Korea Research Institute of Chemical Technology (KRICT), Ulsan 44412, Republic of Korea

[c] Department of Chemistry, Washington University, St. Louis, Missouri, 63130-4899

[d] Department of Chemistry, Korea Advanced Institute of Science and Technology (KAIST), Daejeon 34141, Republic of Korea

[e] Center for Catalytic Hydrocarbon Functionalizations, Institute for Basic Science (IBS), Daejeon 34141, Republic of Korea

[#] These authors contributed equally

[*] Email: mbaik2805@kaist.ac.kr

[*] Email: mirica@illinois.edu

Data Availability Statement

- The data supporting this article have been included as part of the Supplementary Information.
- Crystallographic data for **1** and **2** have been deposited at the Cambridge Crystallographic Data Centre (CCDC) under deposition numbers CCDC 2226270 (**1**) and 2226271 (**2**). These data are provided free of charge by the CCDC (https://www.ccdc.cam.ac.uk/).